

The equation of state and symmetry energy of low density nuclear matter

K. Hagel¹, J. B. Natowitz¹, and G. Röpke²

¹ Cyclotron Institute, Texas A & M University, College Station, Texas 77843-3366, USA

² Institut für Physik, Universität Rostock, Universitätsplatz 3, D-18055 Rostock, Germany

Received: date / Revised version: date

Abstract. The symmetry energy of nuclear matter is a fundamental ingredient in the investigation of exotic nuclei, heavy-ion collisions and astrophysical phenomena. A recently developed quantum statistical (QS) approach that takes the formation of clusters into account predicts low density symmetry energies far above the usually quoted mean field limits. A consistent description of the symmetry energy has been developed that joins the correct low-density limit with values calculated from quasi-particle approaches valid near the saturation density. The results are confronted with experimental values for free symmetry energies and internal symmetry energies, determined at sub-saturation densities and temperatures below 10 MeV using data from heavy-ion collisions. There is very good agreement between the experimental symmetry energy values and those calculated in the QS approach

PACS. 21.65.Ef Symmetry energy – 05.70.Ce Thermodynamic functions and equations of state – 26.60.Kp Equations of state of neutron-star matter – 26.50.+x Nuclear physics aspects of novae, supernovae, and other explosive environments

1 Introduction

Reliable understanding of the density dependence of the nuclear equation of state (EOS) over a wide range of densities and temperatures is a very important need in the investigation of both nuclear and astrophysical phenomena. One fundamental ingredient of the EOS which is the subject of many recent experimental and theoretical investigations is the symmetry energy $E_{\text{sym}}(n, T)$ that describes the dependence of the energy per nucleon on the proton to neutron ratio. It governs phenomena from nuclear structure to astrophysical processes. As a result, the variation of the symmetry energy with nucleon density $n = n_n + n_p$ with n_n, n_p denoting the neutron and proton density, respectively, and temperature T has been extensively investigated in recent years. A recent review is given by Li *et al.* [1]; see also [2] and other contributions to this volume of the European Physical Journal A, in particular [3].

While conventional mean-field approaches to the EOS treat nuclear matter as uniform, it is well established that the properties of low density nuclear matter are governed by correlations, in particular by the appearance of bound states, i.e. clusters. That correlations and clusterization are important and exhibit significant density dependences may be seen, for example, in Figure 1 [4]. In the left side of that figure the calculated density, electron fraction and temperature distributions of a post core collapse supernova are presented as a function of radial distance. At the

larger radii temperatures and densities which are accessible in near Fermi energy collisions [5], are seen. In the right side of the picture are particle mass fractions calculated by Sumiyoshi *et al.* [4] for $Z = 1$ and $Z = 2$ nuclei as a function of radial distance. Furthermore, also the mass fraction of higher mass nuclei (metals) are shown, that is calculated as the sum over all elements with $A > 2$. The role of the cluster formation in the neutrino-sphere region (the region of last neutrino interaction) is of particular interest [6,7]. As will be seen below, this region of temperature and density is accessible in collisions of heavy ions at intermediate energies.

Currently some extensive EOS calculations and existing tabulations, based on varying nucleon-nucleon interactions, serve as standard input for a wide variety of astrophysical simulations. In general these calculations involve a number of simplifying assumptions and allow for a limited number of clustered species at lower densities where important clustering effects are expected [8,9,10,11,12]. We show that new experiments allow for a laboratory test of the EOS and the symmetry energy in the low-density region. The results are in accordance with a systematic QS approach that takes correlations and cluster formation in warm dense matter into account.

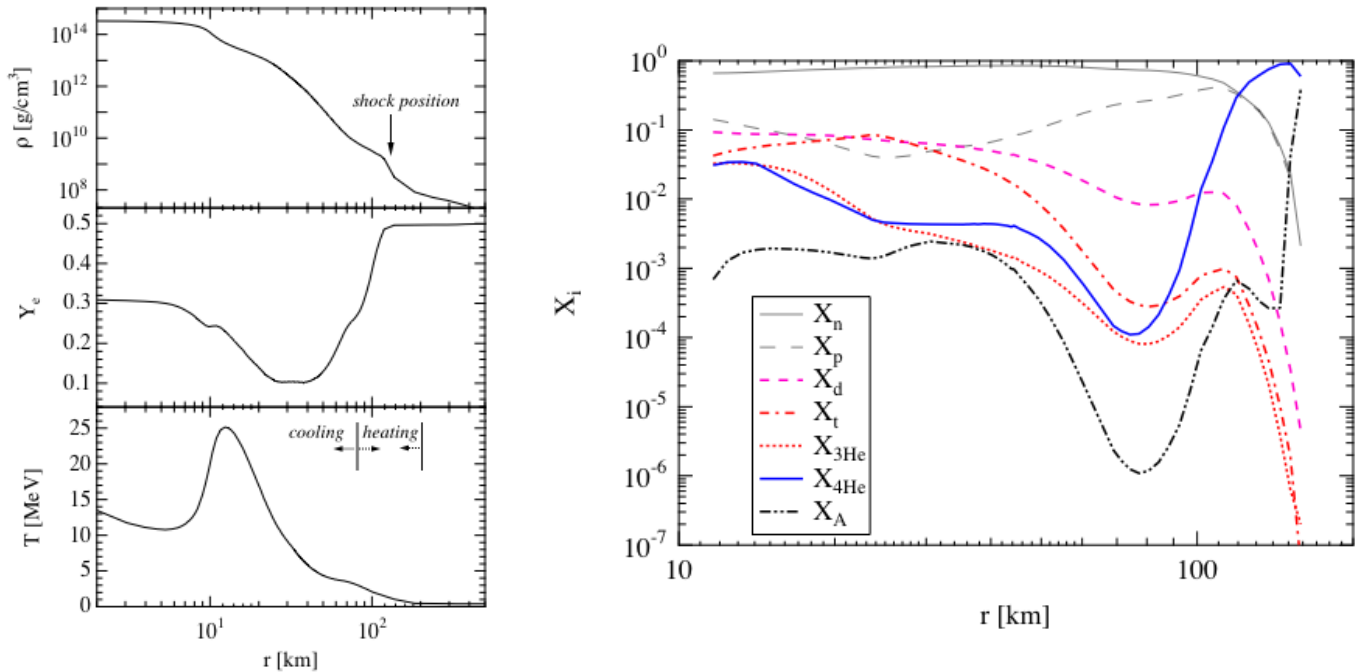


Fig. 1. Left, density, electron fraction and temperature radial profiles of a post core bounce supernova. Right, mass fractions for $Z = 1$ and 2 nuclei as well as $A > 4$ nuclei (metals) as a function of radial distance. See Ref. [4].

2 Clusterization and the symmetry energy at very low density

2.1 Nuclear binding energies and Bethe-Weizsäcker mass formula

The symmetry energy characterizes the dependence of the nuclear binding energy on the asymmetry

$$\delta = (N - Z)/A = 1 - 2Y_p \quad (1)$$

with Z and N the proton and neutron numbers, and $A = N + Z$. In astrophysics, the asymmetry is usually specified by the total proton fraction Y_p . For charge neutral stellar matter Y_p is equal to the electron fraction Y_e . The definition of the symmetry energy can be expressed in different ways, see [3]. Although in the binding energy of nuclei, there is a dependence on δ resulting from the Coulomb interaction, the symmetry energy does not include this trivial effect. Rather, it is defined by the asymmetry contribution of the strong interaction to the binding energy, as expressed within the Bethe-Weizsäcker mass formula

$$B(N, Z) = a_V A - a_S A^{2/3} - \left(a_V^{(\text{sym})} A + a_S^{(\text{sym})} A^{2/3} \right) \delta^2 \quad (2)$$

$$-a_C \frac{Z(Z-1)}{A^{1/3}} + \dots$$

where volume, surface, volume symmetry, surface symmetry and Coulomb contributions exhibit a particular dependence on the mass number A and asymmetry δ . (Pairing and other features such as shell effects are not considered here.) The parameters $a_V, a_S, a_V^{(\text{sym})}, a_S^{(\text{sym})}, a_C$ are generally found by fitting nuclear masses

$$m_{N,Z} = Nm_n + Zm_p - B(N, Z) \quad (3)$$

across the whole chart of known nuclei. Here m_n and m_p are the neutron and proton rest masses, respectively. Typical values of the coefficients $a_V, a_S, a_V^{(\text{sym})}, a_S^{(\text{sym})}, a_C$ are given in Ref. [13].

Our empirical knowledge of the symmetry energy near the saturation density, n_0 , is based primarily on the binding energy analysis. The Bethe-Weizsäcker mass formula leads to values of about $E_{\text{sym}}(n_0, 0) = 28 - 34$ MeV for the nuclear matter symmetry energy at zero temperature and saturation density $n_0 \approx 0.16 \text{ fm}^{-3}$, if surface asymmetry effects are properly taken into account [14]. A recent analysis of experimental data [15] gives the value $a_V^{(\text{sym})} = 32.1 \pm 0.3$ MeV.

Note that in the above, the separation of the Coulomb energy has been performed under the assumption that the strong interaction part is symmetric with respect to $\delta \rightarrow -\delta$ so that the symmetry energy contains no linear term in δ . Then, the Coulomb term in Eq. (2) contains besides the electrostatic field energy also the contribution of the nuclear wave function that may change with the asymmetry δ .

2.2 Symmetry energy of nuclear matter at finite temperature

Within a more fundamental approach, we can consider a given state of the nuclear system described by the wave function ($|\Psi\rangle$) or the statistical operator (ρ) and calculate the expectation value of the energy. In particular, we consider homogeneous matter at finite temperature T consisting of nucleons (neutrons n , protons p) and electrons (e). To eliminate the dependence on the volume V of the system that goes to infinity in the thermodynamic limit, we introduce the neutron density $n_n = N_n/V$ and the proton density $n_p = N_p/V$ that remain finite. The electron density $n_e = n_p$ is necessary to make the system globally charge neutral, to avoid diverging Coulomb energy. It is determined by the proton density and cannot be considered as an additional degree of freedom. Note that we neglect weak interaction processes that lead to β equilibrium so that in full thermodynamic equilibrium the asymmetry (that follows from Eq. (1) after dividing the nucleon numbers by the volume V)

$$\delta = \frac{n_n - n_p}{n}, \quad n = n_n + n_p \quad (4)$$

is an independent thermodynamic parameter, in addition to T and the total baryon density n . We note that the inclusion of further elementary particles such as muons, hyperons or neutrinos may be of interest in astrophysical context, at higher densities and temperatures.

For this "frozen" hot matter characterized by T, n, δ where weak interaction processes are neglected, thermodynamic equilibrium corresponds to the minimum of the free energy

$$\tilde{F}(T, V, N_n, N_p) = V f(T, n, \delta) = N F(T, n, \delta), \quad (5)$$

$N = nV$. To eliminate the dependence on the volume V of the system that goes to infinity, we introduce the density of the free energy $f(T, n, \delta)$ or the free energy per nucleon $F(T, n, \delta) = f(T, n, \delta)/n$. Being a thermodynamic potential, all other thermodynamic quantities such as pressure, entropy or internal energy are consistently derived using the thermodynamic relations.

It is convenient to describe the thermodynamic equilibrium by the grand canonical ensemble that is given by a Gibbs distribution

$$\rho_{\text{gr.can.}}(T, \mu_n, \mu_p) = \frac{1}{Z(T, \mu_n, \mu_p)} e^{-(H - \mu_n N_n - \mu_p N_p)/T} \quad (6)$$

with the neutron chemical potential μ_n and the proton chemical potential μ_p , $Z(T, \mu_n, \mu_p)$ is the partition function. The chemical potential of the background charge compensating electrons is not a new degree of freedom but is fixed by the condition of charge neutrality. As long as there are no phase transitions, the various statistical ensembles are equivalent and give identical results for the equation of state. The chemical potentials are related to the particle densities by the following equations of state

$$\begin{aligned} n_n(T, \mu_n, \mu_p) &= \text{Tr}\{\rho_{\text{gr.can.}}(T, \mu_n, \mu_p) \hat{N}_n\}/V, \\ n_p(T, \mu_n, \mu_p) &= \text{Tr}\{\rho_{\text{gr.can.}}(T, \mu_n, \mu_p) \hat{N}_p\}/V. \end{aligned} \quad (7)$$

In momentum representation, the particle number operators are $\hat{N}_\tau = \sum_{\mathbf{p}, \sigma} a_k^\dagger a_k$ where the quantum number k contains besides momentum \mathbf{p} and spin σ also the isospin τ . We use these thermodynamic relations later on to calculate the free energy by integrating the Helmholtz equation, see Eq. (10) of Ref. [16] and Eq. (23) below.

The Hamiltonian H contains the kinetic energy (we use relativistic kinematics), the strong interaction and the Coulomb interaction that reads in position representation

$$\hat{V}^{\text{Coul}} = \frac{1}{2} \sum_{c,d} \int d^3r \psi_c^\dagger(\mathbf{r}) \psi_d^\dagger(\mathbf{r}') \frac{e_c e_d}{|\mathbf{r} - \mathbf{r}'|} \psi_d(\mathbf{r}') \psi_c(\mathbf{r}) \quad (8)$$

where the index c, d denotes the different components, including spin. Calculating the expectation value of total energy

$$\begin{aligned} U^{\text{total}}(T, V, \mu_n, \mu_p) &= \text{Tr}\{H \rho_{\text{gr.can.}}(T, \mu_n, \mu_p)\} \\ &= U(T, V, \mu_n, \mu_p) + U^{\text{Coul}}(T, V, \mu_n, \mu_p) + U^{\text{el}}(T, V, \mu_n, \mu_p) \end{aligned} \quad (9)$$

for this equilibrium quantum state, one can separate the contribution of the Coulomb energy

$$U^{\text{Coul}} = \text{Tr}\{\rho_{\text{gr.can.}}(T, \mu_n, \mu_p) \hat{V}^{\text{Coul}}\} \quad (10)$$

as well as the contribution of the electron kinetic energy U^{el} . The symmetry energy follows from the expansion of the remaining energy (nucleon kinetic energy and strong interaction) with respect to the asymmetry.

Using the equations of state (7) $n_n = n_n(T, \mu_n, \mu_p)$, $n_p = n_p(T, \mu_n, \mu_p)$ we replace the thermodynamic variables μ_n, μ_p by the densities n_n, n_p or equivalently, the total baryon density n and the asymmetry δ . To obtain the symmetry energy per nucleon we consider the energy per nucleon $E(n, \delta, T) = U(T, V, \mu_n, \mu_p)/N$ (after subtracting the Coulomb energy according to Eq. (9)) as function of δ . Because the strong interaction is assumed to be symmetric with respect to isospin, after subtracting the trivial term due to the difference of the neutron and proton mass in the relativistic kinematics, the first derivative at $\delta = 0$ is approximately zero, so that we have

$$E(n, \delta, T) \approx E(n, 0, T) + (m_n - m_p)\delta + E_{\text{sym}}''(n, T)\delta^2 + \mathcal{O}(\delta^4). \quad (11)$$

Here, the symmetry energy is related to the second derivative with respect to the asymmetry δ . This definition is

appropriate for experimental investigations where we explore nuclei near the valley of stability. In experiments performed for nuclear systems, δ is relatively small.

Another representation of the symmetry energy coefficient is the definition

$$E_{\text{sym}}(n, T) = \frac{E(n, 1, T) + E(n, -1, T)}{2} - E(n, 0, T). \quad (12)$$

This definition is consistent with the use of the second order derivative only if the dependence on δ is purely quadratic. In particular in the case of phase transition and at very low temperatures, this is not exactly the case, see the discussion below and Ref. [3] within this volume.

Comparing with the definition of the symmetry energy for finite nuclei given in the previous subsection, we give some comments. The generalization from ground state nuclei to finite temperatures T is straightforward within the scope of thermodynamics.

An essential topic is the role of the nucleon distribution as expressed by the wave function or the statistical operator. Instead of the equilibrium statistical operator $\rho_{\text{gr.can.}}$, Eq. (6), non-equilibrium distributions can also be considered to investigate the average energy. Some confusion is connected with different assumptions regarding the quantum state of the system, *i. e.* the choice of the wave function ($|\Psi\rangle$) or the statistical operator (ρ). Sometimes an antisymmetrized product ansatz that leads to the mean-field approximation is taken. However, this ansatz, appropriate for noninteracting fermion systems, is not correct in describing the ground state or the thermodynamic equilibrium at finite T for the interacting nuclear system because all correlations are neglected. To treat real systems, for instance in astrophysics, we have to take into account the correlations that are also present at thermodynamic equilibrium and are determined by the full Hamiltonian H .

More delicate is the subdivision of the symmetry energy in Eq. (2) into a volume part and a surface part. For homogeneous systems, the density does not depend on the position in coordinate space. This is also correct for correlations and bound state formation if the center-of-mass motion is taken into account. Correlations and bound state formation are seen in the two-particle distribution function (structure factor). After separation of the center-of-mass motion, the internal wave function of a cluster is usually approximated within a local-density approach. Thomas-Fermi models, droplet models, and gradient expansions can be applied to estimate the binding energy of a cluster. Thus, the definition of the symmetry energy (11) is not in conflict with the Bethe-Weizsäcker formula (2) that follows if the distribution of clusters (nuclei) is given ("frozen out"). Neglecting the center-of-mass motion, the internal density distribution of the cluster can be treated within a gradient expansion that gives, within the local density approximation, the volume term and the surface term. However, this subdivision, that is useful for some approximations, is not rigorous and cannot be applied, for instance, to describe the contribution of light clusters such as deuterons or α particles.

We also note that in the uncorrelated state of symmetric nuclear matter, where cluster formation is neglected (or the strong interaction is dropped), the Coulomb energy for charge neutral matter (proton and electron densities constant and compensating) does not vanish. Only the Hartree term is zero. Because of microfield fluctuations there is also a finite value of the Coulomb energy. In the lowest approximation we obtain the Debye shift due to the two-particle distribution function (Montroll - World contribution to the virial expansion of the equation of state), see for instance Ref. [17].

The Coulomb interaction occurs in two positions: the energy that is clearly additive and can be separated, and the influence on the quantum state or structure that is given, for instance, by the equilibrium distribution or the ground state wave function. Without Coulomb interactions, the structure of nuclei would change significantly and would lead to arbitrarily large stable nuclei what is not realistic. Also the two-phase separation that is obtained considering only strong interaction is disfavored because of large Coulomb energy what leads to so-called pasta structures. (Note that due to the Hamiltonian that is used to describe the ground state or thermodynamic equilibrium, the Coulomb interaction also indirectly leads to a linear term $\propto \delta$ in the energy that can be compensated by a redefinition of the Coulomb term.)

2.3 The symmetry energy at sub-saturation densities

We introduce the symmetry energy of nuclear matter at finite temperature to characterize the properties of matter in astrophysics or in excited nuclei. To describe real systems, the quantum statistical approach is used to introduce well-defined quantities. Then, special approximations can be performed that may lead to different results, due to the approximations used. Thus, different results for the symmetry energy of nuclear matter can be found in the literature that describe experiments with real systems to a good approximation only if the relevant processes are taken into account. In the case of the symmetry energy of low density nuclear matter considered here, correlations and cluster formation are essential and have to be taken into account. Mean-field approaches such as Skyrme interaction or relativistic mean field (RMF) approximation are not able to describe adequately the quantum state of matter at low densities because all correlations are neglected. Most of recently used treatments do not give the correct low-density limit that is governed by cluster formation, as discussed in the following subsection.

Two different pictures are used to describe nuclear matter at sub-saturation densities. Near the saturation density, n_0 , the Fermi-liquid (single quasiparticle) approach is used to describe nuclear systems. This picture is confined to that region where correlations, in particular cluster formation, are not relevant. To give a number, the density should be larger than $n_0/3$. An alternative picture for hot nuclear systems is nuclear statistical equilibrium (NSE) and related models that treat a noninteracting gas

consisting of all possible bound states in chemical equilibrium (mass action law). This chemical picture is confined to the low-density region (below $5 \times 10^{-4} \text{ fm}^{-3}$) where the interaction between the constituents can be neglected.

Many theoretical investigations have been performed to estimate the behavior of the symmetry energy as a function of n and T (Li *et al.* [1], see also [18,19]). Typically, quasi-particle approaches such as Skyrme Hartree-Fock and relativistic mean field (RMF) models or Dirac-Brueckner Hartree-Fock calculations are used. The uniform matter symmetry energy obtained in this approximation goes linearly to zero when the density goes to zero,

$$E_{\text{sym}}(n, T) \propto n. \quad (13)$$

Such a behavior is often seen in the results shown in the literature, but is incorrect because correlations are not included.

At low density the symmetry energy changes mainly because additional binding is gained in symmetric matter due to formation of clusters and pasta structures [20]. Therefore, the symmetry energy in the low-temperature limit has to be equal to the binding energy per nucleon associated with the strong interaction of the most bound nuclear cluster. Theoretical calculations of the density dependence of the symmetry energy based on conventional mean-field approaches and ignoring cluster formation will fail to give the correct low-temperature, low-density limit to the symmetry energy. The correct low-density limit can be recovered only if the formation of clusters is properly taken into account, as has previously been shown in Ref. [21], see also [12,22] in the context of a virial expansion valid at very low densities, and in Ref. [16].

Approaches used to account for cluster formation include the nuclear statistical equilibrium model (NSE) [23], cluster-virial expansions [12], as well as generalized Beth-Uhlenbeck approaches [22]. A thermodynamic Green's function approach that allows a generalization of the NSE model by introducing a quasiparticle description also for the bound states was already formulated some decades ago [21], but only recently analyzed with respect to the experimental consequences for nuclear matter [24].

To deal with the clusterization, we employ a quantum statistical (QS) approach which takes into account cluster correlations in the medium. To extend the range of applicability of this approach, we then interpolate between the exact low-density limit and the very successful RMF approaches near the saturation density to provide a representation useful over a wide range of densities.

In this QS approach cluster correlations are described in a generalized Beth-Uhlenbeck expansion. The advantage of this method is that the medium modifications of the clusters at finite density are taken into account. In Ref. [16] the thermodynamic properties of nuclear matter were derived using this approach. The formulation of Ref. [16] is valid in the density and temperature range where the formation of light clusters with $A \leq 4$ dominates and heavier clusters are not yet important. The method requires a reasonably accurate modeling of the quasiparticle properties. For that we employ a RMF model with

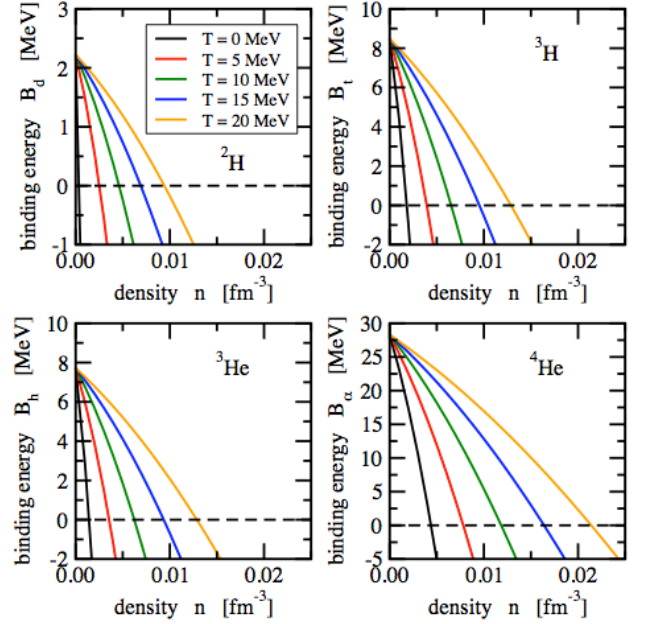


Fig. 2. Change of the binding energy $B_i = -E_i^0$ of the clusters $i = d, t, h, \alpha$ at rest in symmetric nuclear matter due to the binding energy shift B_i as used in the generalized RMF model as a function of the total nucleon density n . Mott points for specific temperature-density combinations appear when the binding energy relative to the medium becomes $= 0$.

density dependent couplings [25] which gives a good description both of nuclear matter around normal density and of ground state properties of nuclei across the nuclear chart. In order to extend the applicability of this RMF model to very low densities, it has been generalized in Ref. [16] to account also for cluster formation and destruction. The model allows derivation of the composition and the thermodynamic quantities of nuclear matter can be modeled in a large region of densities, temperatures and asymmetries that are required, for example, in supernova simulations.

This generalized model naturally leads to a decrease of the cluster mass fractions at high densities, reflecting a reduction of the cluster binding energies due to Pauli blocking. The binding energy of a cluster relative to the medium vanishes at a point known as the Mott point. As a result, well-defined clusters appear for densities below approximately 1/10 of the saturation density and get dissolved at higher densities. (Because of the presence of strong correlations in the scattering state continuum that are effectively represented by one resonance, there is a diminishing but non vanishing cluster fraction above the Mott density.) The Mott point is temperature dependent as seen in Figure 2 where calculated Mott points for $d, t, {}^3\text{He}$ and α particles are represented [16].

3 Quantum statistical approach to the symmetry energy of nuclear matter at finite temperature

3.1 General approach

To describe the thermodynamic properties of a many-particle system, the thermodynamic (Matsubara) Green's function approach can be used. Exact expressions for the equations of state (7) can be given that contain the single-particle spectral function $S_\tau(\mathbf{p}, \omega)$,

Using the finite-temperature Green function formalism, a non-relativistic quantum statistical approach can be given to describe the equation of state of nuclear matter including the formation of bound states [21, 22]. It is most convenient to start with the nucleon number densities $n_\tau(T, \mu_p, \mu_n)$ as functions of temperature T and non-relativistic chemical potentials μ_τ for protons ($\tau = p$) and neutrons ($\tau = n$), respectively,

$$n_\tau(T, \mu_p, \mu_n) = 2 \int \frac{d^3 k_1}{(2\pi)^3} \int_{-\infty}^{\infty} \frac{d\omega}{2\pi} f_{1,Z}(\omega) S_\tau(1, \omega). \quad (14)$$

Summation over spin yields the factor 2 and

$$f_{A,Z}(\omega) = \left(\exp \{ \beta [\omega - Z\mu_p - (A-Z)\mu_n] \} - (-1)^A \right)^{-1} \quad (15)$$

is the Fermi or Bose distribution function which depends on the inverse temperature $\beta = 1/T$. Instead of the isospin quantum number τ we occasionally use the mass number A and the charge number Z . Both the distribution function and the spectral function $S_1(1, \omega)$ depend on the temperature and the chemical potentials μ_p, μ_n not given explicitly. For this EOS (14), expressions such as the Beth-Uhlenbeck formula and its generalizations have been derived [12, 21, 22].

The spectral function $S_\tau(1, \omega)$ is related to the self-energy $\Sigma(1, z)$ according to

$$S_\tau(1, \omega) = \frac{2\text{Im} \Sigma(1, \omega - i0)}{[\omega - E(1) - \text{Re} \Sigma(1, \omega)]^2 + [\text{Im} \Sigma(1, \omega - i0)]^2}, \quad (16)$$

where the imaginary part has to be taken for a small negative imaginary part in the frequency ω . $E(1) = p^2/(2m)$ is the kinetic energy of the free nucleon. The solution of the relation

$$E_1^{\text{qu}}(1) = E(1) + \text{Re} \Sigma[1, E_1^{\text{qu}}(1)] \quad (17)$$

defines the single-nucleon quasiparticle energies $E_1^{\text{qu}}(1) = E(1) + \Delta E^{\text{SE}}(1)$. Expanding for small $\text{Im} \Sigma(1, z)$, the spectral function yields a δ -like contribution. The densities are calculated from Fermi distributions with the quasiparticle energies so that

$$n_\tau^{\text{qu}}(T, \mu_p, \mu_n) = \frac{2}{V} \sum_{k_1} f_{1,Z}[E_1^{\text{qu}}(1)] \quad (18)$$

follows for the EOS in mean field approximation. This result does not contain the contribution of bound states

and therefore is not correct in the low-temperature, low-density limit where the NSE describes the nuclear matter EOS.

As shown in Refs. [21, 22], the bound state contributions are obtained from the poles of $\text{Im} \Sigma(1, z)$ which cannot be neglected in expanding the spectral function with respect to $\text{Im} \Sigma(1, z)$. A cluster decomposition of the self-energy has been proposed, see [21]. The self-energy is expressed in terms of the A -particle Green functions which read in bilinear expansion

$$G_A(1 \dots A, 1' \dots A', z_A) = \sum_{\nu K} \psi_{A\nu K}(1 \dots A) \times \frac{1}{z_A - E_{A,\nu}^{\text{qu}}(K)} \psi_{A\nu K}^*(1' \dots A'). \quad (19)$$

The A -particle wave function $\psi_{A\nu K}(1 \dots A)$ and the corresponding eigenvalues $E_{A,\nu}^{\text{qu}}(K)$ result from solving the in-medium Schrödinger equation, see the following Subsections. K denotes the center of mass momentum of the A -nucleon system. Besides the bound states, the summation over the internal quantum states ν includes also the scattering states.

The evaluation of the equation of state in the low-density limit is straight forward. Considering only the bound-state contributions, we obtain the result

$$n_p^{\text{tot}}(T, \mu_p, \mu_n) = \frac{1}{V} \sum_{A,\nu,K} Z f_{A,Z}[E_{A,\nu}^{\text{qu}}(K; T, \mu_p, \mu_n)], \quad (20)$$

$$n_n^{\text{tot}}(T, \mu_p, \mu_n) = \frac{1}{V} \sum_{A,\nu,K} (A-Z) f_{A,Z}[E_{A,\nu}^{\text{qu}}(K; T, \mu_p, \mu_n)]$$

for the EOS describing a mixture of components (cluster quasiparticles) obeying Fermi or Bose statistics. The total baryon density results as $n(T, \mu_p, \mu_n) = n_p^{\text{tot}}(T, \mu_p, \mu_n) + n_n^{\text{tot}}(T, \mu_p, \mu_n)$. To derive the extended Beth-Uhlenbeck formula, see [22], we restrict the summation to $A \leq 2$, but extend the summation over the internal quantum numbers ν , not only to the excited states, but also the scattering states. Note that at low temperatures Bose-Einstein condensation may occur.

The NSE is obtained in the low-density limit if the in-medium energies $E_{A,\nu}^{\text{qu}}(K; T, \mu_p, \mu_n)$ can be replaced by the binding energies of the isolated nuclei $E_{A,\nu}^{(0)}(K) = E_{A,\nu}^{(0)} + K^2/(2Am)$, with $m = 939$ MeV the average nucleon mass. For the cluster contributions, i.e. $A > 1$, the summation over the internal quantum numbers is again restricted to the bound states only. We have

$$n_p^{\text{NSE}}(T, \mu_p, \mu_n) = \frac{1}{V} \sum_{A,\nu,K}^{\text{bound}} Z f_{A,Z}[E_{A,\nu}^{(0)}(K)], \quad (21)$$

$$n_n^{\text{NSE}}(T, \mu_p, \mu_n) = \frac{1}{V} \sum_{A,\nu,K}^{\text{bound}} (A-Z) f_{A,Z}[E_{A,\nu}^{(0)}(K)].$$

The summation over A includes also the contribution of free nucleons, $A = 1$.

In the nondegenerate and nonrelativistic case assuming a Maxwell-Boltzmann distribution, the summation over the momenta K can be performed analytically and the thermal wavelength $\Lambda = \sqrt{2\pi/(mT)}$ of the nucleon occurs. As shown below, the medium effects in nuclear matter are negligible below 10^{-4} times the saturation density n_0 for the temperatures considered here.

Interesting quantities are the mass fractions

$$X_{A,Z} = \frac{A}{Vn} \sum_{\nu,K} f_{A,Z}[E_{A,\nu}^{\text{qu}}(K; T, \mu_p, \mu_n)] \quad (22)$$

of the different clusters. From the EOS considered here, thermodynamical potentials can be obtained by integration, in particular the free energy per volume $f = \bar{F}/V$. In the special case of symmetric nuclear matter, $Y_p^s = 0.5$, the free energy per volume is obtained from the averaged chemical potential $\mu = (\mu_p + \mu_n)/2$ (symmetric matter) as

$$f(T, n, Y_p^s) = \int_0^n dn' \mu(T, n', Y_p^s). \quad (23)$$

In the quantum statistical approach described above, we relate the EOS to properties of the correlation functions, in particular to the peaks occurring in the A -nucleon spectral function describing the single-nucleon quasiparticle ($A = 1$) as well as the nuclear quasiparticles ($A \geq 2$). The microscopic approach to these quasiparticle energies can be given calculating the self-energy. Different approaches can be designed which reproduce known properties of the nucleonic system.

3.2 Medium modification of single nucleon properties

The single-particle spectral function contains the single-nucleon quasiparticle contribution, $E_1^{\text{qu}}(1) = E_\tau^{\text{qu}}(k)$, given in Eq. (17), where τ denotes isospin of particle 1 and k is the momentum. In the effective mass approximation, the single-nucleon quasiparticle dispersion relation reads

$$E_\tau^{\text{qu}}(k) = \Delta E_\tau^{\text{SE}}(0) + \frac{k^2}{2m_\tau^*} + \mathcal{O}(k^4), \quad (24)$$

where the quasiparticle energies are shifted at zero momentum k by $\Delta E_\tau^{\text{SE}}(0)$, and m_τ^* denotes the effective mass of neutrons ($\tau = n$) or protons ($\tau = p$). Both quantities, $\Delta E_\tau^{\text{SE}}(0)$ and m_τ^* , are functions of T , n_p and n_n , characterizing the surrounding matter.

Expressions for the single-nucleon quasiparticle energy $E_\tau^{\text{qu}}(k)$ can be given by the Skyrme parametrization [27] or by more sophisticated approaches such as relativistic mean-field (RMF) approaches [25], and relativistic Dirac-Brueckner Hartree-Fock [18] calculations. We use the density-dependent relativistic mean field approach of [25] that is designed not only to reproduce known properties of nuclei, but also fits with microscopic calculations in the low density region.

We can assume [19] that the density-dependent RMF parametrisation covers a large density region. It will be

used in this work to determine the single-nucleon quasiparticle energies. The single-nucleon quasiparticle energies result as

$$E_{n,p}^{\text{qu}}(0) = \sqrt{[m^2 - S(T, n, \pm\delta)]^2 + k^2} + V(T, n, \pm\delta). \quad (25)$$

In the nonrelativistic limit, the shifts of the quasiparticle energies are

$$\Delta E_{n,p}^{\text{SE}}(k) = V(T, n, \pm\delta) - S(T, n, \pm\delta). \quad (26)$$

The effective masses for neutrons and protons are given by

$$m_{n,p}^* = m - S(T, n, \pm\delta). \quad (27)$$

Approximations for the functions $V(T, n, \delta)$ and $S(T, n, \delta)$ are given in the literature [26]. These functions reproduce the empirical values for the saturation density $n_0 \approx 0.15 \text{ fm}^{-3}$ and the binding energy per nucleon $B/A \approx -16 \text{ MeV}$. The effective mass is somewhat smaller than the empirical value $m^* \approx m(1 - 0.17 n/n_0)$ for $n < 0.2 \text{ fm}^{-3}$.

3.3 Medium modification of cluster properties

Recent progress of the description of clusters in low density nuclear matter [4, 24, 28] enables us to evaluate the properties of deuterons, tritons, helions and helium nuclei in a non-relativistic microscopic approach, taking the influence of the medium into account.

In addition to the δ -like nucleon quasiparticle contribution, also the contribution of the bound and scattering states can be included in the single-nucleon spectral function by analyzing the imaginary part of $\Sigma(1, z)$. Within a cluster decomposition, A -nucleon T matrices appear in a many-particle approach. These T matrices describe the propagation of the A -nucleon cluster in nuclear matter. In this way, bound states contribute to $n_\tau = n_\tau(T, \mu_n, \mu_p)$, see [21, 22]. Restricting the cluster decomposition only to the contribution of two-particle correlations, we obtain the so-called T_2G approximation. In this approximation, the Beth-Uhlenbeck formula is obtained for the EOS, as shown in [21, 22]. In the low-density limit, the propagation of the A -nucleon cluster is determined by the energy eigenvalues of the corresponding nucleus, and the simple EOS (20) results describing the nuclear statistical equilibrium (NSE).

For nuclei imbedded in nuclear matter, an effective wave equation can be derived [21, 24]. The A -particle wave function $\psi_{A\nu K}(1 \dots A)$ and the corresponding eigenvalues $E_{A,\nu}^{\text{qu}}(K)$ follow from solving the in-medium Schrödinger equation

$$\begin{aligned} & [E^{\text{qu}}(1) + \dots + E^{\text{qu}}(A) - E_{A,\nu}^{\text{qu}}(K)] \psi_{A\nu K}(1 \dots A) \\ & + \sum_{1' \dots A'} \sum_{i < j} [1 - \tilde{f}(i) - \tilde{f}(j)] V(ij, i'j') \\ & \times \prod_{k \neq i,j} \delta_{kk'} \psi_{A\nu K}(1' \dots A') = 0. \end{aligned} \quad (28)$$

This equation contains the effects of the medium in the single-nucleon quasiparticle shifts as well as in the Pauli

blocking terms. The A -particle wave function and energy depend on the total momentum K relative to the medium.

The in-medium Fermi distribution function $\tilde{f}(1) = (\exp\{\beta[E^{\text{qu}}(1) - \tilde{\mu}_{\tau_1}]\} + 1)^{-1}$ contains the non-relativistic effective chemical potential $\tilde{\mu}_{\tau}$ which is determined by the total proton or neutron density calculated in quasiparticle approximation, $n_{\tau}^{\text{tot}} = V^{-1} \sum_1 \tilde{f}(1) \delta_{\tau_1, \tau}$ for the particles inside the volume V . It describes the occupation of the phase space neglecting any correlations in the medium. The solution of the in-medium Schrödinger equation (28) can be obtained in the low-density region by perturbation theory. In particular, the quasiparticle energy of the A -nucleon cluster with Z protons in the ground state follows as

$$E_{A,\nu}^{\text{qu}}(K) = E_{A,Z}^{(0)} + \frac{K^2}{2Am} + \Delta E_{A,Z}^{\text{SE}}(K) + \Delta E_{A,Z}^{\text{Pauli}}(K) + \Delta E_{A,Z}^{\text{Coul}}(K), \quad (29)$$

plus higher order contributions with respect to density. Besides the cluster binding energy in the vacuum $E_{A,Z}^{(0)}$ and the kinetic term, the self-energy shift $\Delta E_{A,Z}^{\text{SE}}(K)$, the Pauli shift $\Delta E_{A,Z}^{\text{Pauli}}(K)$ and the Coulomb shift $\Delta E_{A,Z}^{\text{Coul}}(K)$ enter. The latter can be evaluated for dense matter in the Wigner-Seitz approximation [29,30,31]. It is given by

$$\Delta E_{A,Z}^{\text{Coul}}(K) = \frac{Z^2}{A^{1/3}} \frac{3e^2}{5r_0} \left[\frac{3}{2} \left(\frac{2n_p}{n_0} \right)^{\frac{1}{3}} - \frac{n_p}{n_0} \right] \quad (30)$$

with $r_0 = 1.2$ fm. Since the values of Z are small, this contribution is small as well and disregarded here together with other small higher order terms in the quasiparticle energy (29).

The self-energy contribution to the quasiparticle shift is determined by the contribution of the single-nucleon shift

$$\Delta E_{A,Z}^{\text{SE}}(0) = (A-Z)\Delta E_n^{\text{SE}}(0) + Z\Delta E_p^{\text{SE}}(0) + \Delta E_{A,Z}^{\text{SE,eff.mass}}. \quad (31)$$

The contribution to the self-energy shift due to the change of the effective nucleon mass can be calculated from perturbation theory using the unperturbed wave function of the clusters, see [4], so that

$$\Delta E_{A,Z}^{\text{SE,eff.mass}} = \left(\frac{m}{m^*} - 1 \right) s_{A,Z}. \quad (32)$$

Values of $s_{A,Z}$ for $\{A, Z\} = \{i\} = \{d, t, h, \alpha\}$ are given in Ref. [16]. Inserting the medium-dependent quasiparticle energies in the distribution functions (15) this contribution to the quasiparticle shift can be included renormalizing the chemical potentials.

The most important effect in the calculation of the abundances of light elements comes from the Pauli blocking terms in Eq. (28) in connection with the interaction potential. This contribution is restricted only to the bound states so that it may lead to the dissolution of the nuclei if the density of nuclear matter increases. The corresponding shift $\Delta E_{A,Z}^{\text{Pauli}}(K)$ can be evaluated in perturbation theory

provided the interaction potential and the ground state wave function are known. After angular averaging where in the Fermi functions the mixed scalar product $\mathbf{k} \cdot \mathbf{K}$ between the total momentum \mathbf{K} and the remaining Jacobian coordinates \mathbf{k} is neglected, the Pauli blocking shift can be approximated as

$$\Delta E_{A,Z}^{\text{Pauli}}(K) \approx \Delta E_{A,Z}^{\text{Pauli}}(0) \exp\left(-\frac{K^2}{g_{A,Z}}\right) \quad (33)$$

where the amplitude $\Delta E_{A,Z}^{\text{Pauli}}(0)$ and the dispersion g_i depend on the thermodynamic parameters (T, n, Y_p) . Values are given in [16], for a more recent calculation see [24,32].

With the neutron number $N_i = A_i - Z_i$, it can be written as

$$\Delta E_{A_i, Z_i}^{\text{Pauli}}(0; n_p, n_n, T) = -\frac{2}{A_i} [Z_i n_p + N_i n_n] \delta E_i^{\text{Pauli}}(T, n), \quad (34)$$

where the temperature dependence and higher density corrections are contained in the functions $\delta E_i^{\text{Pauli}}(T, n)$.

Now, the nucleon number densities (21) can be evaluated as in the non-interacting case, with the only difference that the number densities of the particles are calculated with the quasiparticle energies. In the light cluster-quasiparticle approximation, the total densities of neutrons (note that we change the notation to distinguish between the total nucleon density, former n_{τ} , and the free nucleon density)

$$n_n^{\text{tot}} = n_n + \sum_{i=d,t,h,\alpha} N_i n_i \quad (35)$$

and of protons

$$n_p^{\text{tot}} = n_p + \sum_{i=d,t,h,\alpha} Z_i n_i \quad (36)$$

contain the densities of the free neutrons and protons n_n and n_p , respectively, and the contributions from the nucleons bound in the clusters with densities n_i . The state of the system in chemical equilibrium is completely determined by specifying the total nucleon density $n = n_n^{\text{tot}} + n_p^{\text{tot}}$, the asymmetry δ and the temperature T as long as no β -equilibrium is considered.

This result is an improvement of the NSE and allows for the smooth transition from the low-density limit up to the region of saturation density. The bound state contributions to the EOS are fading with increasing density because they move as resonances into the continuum of scattering states. This improved NSE, however, does not contain the contribution of scattering states explicitly. For the treatment of continuum states in the two-nucleon case, as well as the evaluation of the second virial coefficient, see [12,22].

The account of scattering states needs further consideration. Investigations on the two-particle level have been performed and extensively discussed [12,21,22]. We use the Levinson theorem to take the contribution of scattering states into account in the lowest-order approximation. Each bound state contribution to the density has to

accompanied with a continuum contribution that partly compensates the strength of the bound state correlations. As a consequence, the total proton and neutron densities are given by

$$n_p^{\text{tot}}(T, \mu_p, \mu_n) = \frac{1}{V} \sum_{A, \nu, K}^{\text{bound}} Z \left[f_{A, Z}[E_{A, \nu}^{\text{qu}}(K; T, \mu_p, \mu_n)] - f_{A, Z}[E_{A, \nu}^{\text{cont}}(K; T, \mu_p, \mu_n)] \right], \quad (37)$$

$$n_n^{\text{tot}}(T, \tilde{\mu}_p, \tilde{\mu}_n) = \frac{1}{V} \sum_{A, \nu, K}^{\text{bound}} (A - Z) \left[f_{A, Z}[E_{A, \nu}^{\text{qu}}(K; T, \mu_p, \mu_n)] - f_{A, Z}[E_{A, \nu}^{\text{cont}}(K; T, \mu_p, \mu_n)] \right] \quad (38)$$

with explicit bound and scattering terms. $E_{A, \nu}^{\text{cont}}$ denotes the edge of the continuum states that is also determined by the single-nucleon self-energy shifts. These expressions guarantee a smooth behavior if bound states merge with the continuum of scattering states. The summation over A includes also the contribution of free nucleons, $A = 1$, considered as quasiparticles with the energy dispersion given by the RMF approach.

The summation over K and the subtraction of the continuum contribution is extended only over that region of momentum space where bound states exist. The disappearance of the bound states is caused by the Pauli blocking term; the self-energy contributions to the quasiparticle shifts act on bound as well as on scattering states. Above the so-called Mott density, where the bound states at $K = 0$ disappear, the momentum summation has to be extended only over that region $K > K_{A, \nu}^{\text{Mott}}(T, n, \delta)$ where the bound state energy is lower than the continuum of scattering states. The contribution of scattering states is necessary to obtain the second virial coefficient according to the Beth-Uhlenbeck equation, see [12, 22]. This leads also to corrections in comparison with the NSE that accounts only for the bound state contributions, neglecting all effects of scattering states. These corrections become important at increasing temperatures for weakly bound clusters. Thus, the corrections which lead to the correct second virial coefficient are of importance for the deuteron system, when the temperature is comparable or large compared with the binding energy per nucleon. In the calculations for the quantum statistical (QS) model shown below, the contributions of these continuum correlations have been taken into account.

Solving Eqs. (37) and (38) for given T , n_p^{tot} and n_n^{tot} we find the chemical potentials μ_p and μ_n . After integration, see Eq. (23), the free energy is obtained, and all the other thermodynamic functions are derived from this quantity without any contradictions. Results are given below.

We do not consider the formation of heavy clusters here. This limits the parameter range n_n^{tot} , n_p^{tot} , T in the phase diagram to that area where the abundances of heavier clusters are small. For a more general approach to the EOS which takes also the contribution of heavier cluster into account, see [29]. Future work will include the contribution of the heavier clusters.

Further approximations refer to the linear dependence on density of the shifts of binding energies, calculated in perturbation theory. A better treatment will improve these shifts, but it can be shown that the changes are small. Furthermore, the approximation of the uncorrelated medium can be improved considering the cluster mean-field approximation [21, 24, 33]. Last but not least, the formation of quantum condensates will give further contributions to the EOS. However, in the region considered here the formation of quantum condensates does not appear.

3.4 Results for the symmetry energy

We perform the calculations for $A \leq 4$ and compare them with several approximations. Solving the EOS (37), (38), we find the chemical potentials for symmetric matter as function of the densities and the temperature. The free energy density is obtained after integration, and the internal energy follows from the standard thermodynamic relations. The same procedure is made for neutron matter, and the difference of the internal energies gives the symmetry energy as shown in Figures 3 and 4. The symmetry energy is calculated by using the finite difference formula, Eq. (12). The Coulomb energy of the clusters has been subtracted. Cluster formation is more clearly seen in the logarithmic scale, Fig. 3, whereas the linear scale, Fig. 4, is commonly used. The disappearance of clusters around $n_0/5$ indicates the transition to the RMF result. Because of the temperature dependence of the composition, the symmetry energy that is determined by the yields of clusters also depends strongly on T .

Degeneration effects are small, but can be easily incorporated. At low temperatures and high densities nucleons follow Fermi statistics. Pairing occurs in the two-nucleon channel and the transition from Cooper pairing to Bose-Einstein condensation is included. Even more interesting is Bose condensation for larger bosonic bound states that may occur at very low temperatures. The quarteting is a possible contribution that is presently not included.

This analysis should be improved by further considering the effects of continuum correlations. In particular, this will affect the contribution of deuterons that are weakly bound, and has been already taken into account in the present calculation. The Beth-Uhlenbeck formula gives the exact expression for the second virial coefficient. The effects become more relevant for high temperatures.

Due to the formation of correlations, in particular clusters, the symmetry energy becomes strongly temperature dependent. For decreasing temperatures, the contribution of higher clusters $A > 4$ is increasing. For an estimate of the contribution of higher clusters see [3, 11]. Charge-neutral nuclear matter will not show a first order phase transition because of the Coulomb interaction that gives diverging energy, if with a homogeneous background of electrons the nuclear matter disassembles into a liquid phase and a gas-like phase. In that region, droplets and pasta-like structures may be formed, that are not fixed in space. Thus, the system remains in a homogeneous state

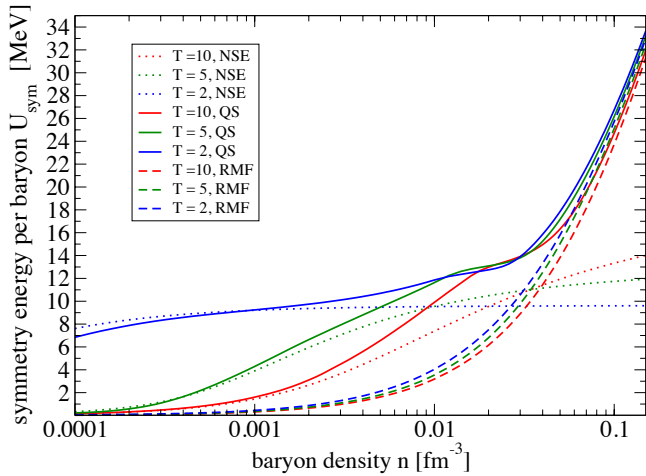


Fig. 3. QS calculation of internal symmetry energy as function of baryon density n for different temperatures. For comparison, the NSE and RMF approximations are also given.

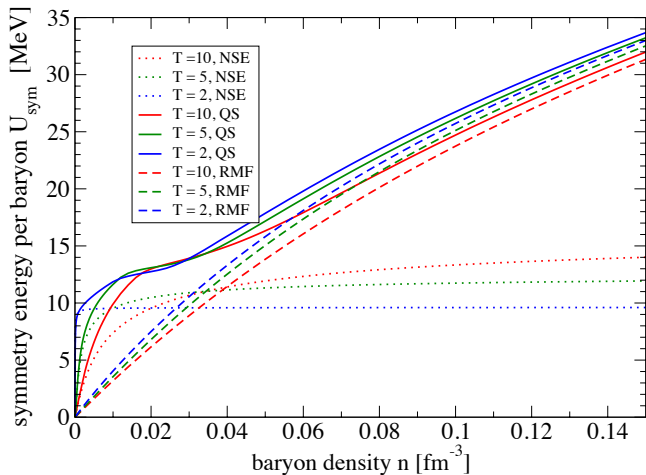


Fig. 4. The same as Fig. 3, linear density scale.

in the thermodynamic context with a constant average density.

4 Laboratory Tests of the Equation of State at Low Density

4.1 Experimental Technique

The experimental information is derived from heavy-ion collisions of charge asymmetric nuclei, where transient states of different density can be reached, depending on the incident energy and the centrality of the collision.

In the Fermi energy domain effects of the symmetry energy have been investigated in judiciously chosen observables [1, 34] suggesting an almost linear behavior around and below normal density [35, 36, 37].

Our experimental investigations of low density nuclear matter have utilized near Fermi energy heavy ion collisions to produce heated and expanded matter [5, 38, 39, 40, 41]. Cluster production was studied using the 4π multi-detector, NIMROD, at the Cyclotron Institute at Texas A&M University. NIMROD consists of a 166 segment charged particle array set inside a neutron ball [42]. The charged particle array is arranged in 12 rings of Si-CsI telescopes or single CsI detectors concentric around the beam axis. The CsI detectors are 1-10 cm thick Tl doped crystals read by photomultiplier tubes. A pulse shape discrimination method is employed to identify light particles in the CsI detectors. For this experiment each of the forward rings included two segments having two Si detectors (150 and 500 μm thick) in front of the CsI detectors (super telescopes) and three having one Si detector (300 μm thick). Each super telescope was further divided into two sections. Neutron multiplicity was measured with the 4π neutron detector surrounding the charged particle array. This detector is a neutron calorimeter filled with Gd doped pseudocumene. Thermalization and capture of emitted neutrons in the ball leads to scintillation which is observed with phototubes providing event by event determination of neutron multiplicities. Further details on the detection system, energy calibrations and neutron ball efficiency may be found in Ref. [43, 44]. The combined neutron and charged particle multiplicities were employed to select the most violent events for subsequent analysis.

Analyzing heavy ion collisions using the NIMROD multi-detector at Texas A&M University, the medium modification of light fragments that leads to the dissolution has been shown. Yields of light particles produced in the collisions of 47 A MeV ^{40}Ar with ^{112}Sn , ^{124}Sn and ^{64}Zn with ^{112}Sn , ^{124}Sn were employed in Thermal coalescence model analyses to derive densities and temperatures of the evolving emitting systems. Free symmetry energies of these systems were determined using Isoscaling analyses.

The light particles and clusters emitted at the early stage of such collision are messengers carrying information on the dynamic evolution of the system and its degree of equilibration. We measure their energies, angles and yields and use that information to probe the properties of the system. We do this as a function of surface velocity of the emitted species. The surface velocity v_{surf} , i.e. the velocity before the final Coulomb acceleration, serves as a surrogate to follow the time evolution of the system [45].

Experimental determinations of the symmetry energy at very low densities produced in heavy ion collisions of ^{64}Zn on ^{92}Mo and ^{197}Au at 35 MeV per nucleon have also been reported [5]. The surface velocity was also used as a measure of the time when the particles leave the source under different conditions of density and temperature. Only values of $v_{\text{surf}} < 4.5$ cm/ns were included in that work since it was argued that the system does not reach equilibrium for higher v_{surf} , see Tab. I of Ref. [5].

Another experiment [46,47] was performed to study the dependence of the thermodynamic properties of nuclear material on neutron-proton asymmetry [48]. Here, collisions of $^{70}\text{Zn}+^{70}\text{Zn}$, $^{64}\text{Zn}+^{64}\text{Zn}$, and $^{64}\text{Ni}+^{64}\text{Ni}$ at $E/A = 35$ MeV were studied. Charged particles and free neutrons produced in the reactions were measured in the NIMROD-ISiS 4π detector array [42,49]. The energy resolution achieved allowed excellent isotopic resolution of charged particles up to $Z = 17$. For events in which all charged particles are isotopically identified, the QP (quasi-projectile, the primary excited fragment that exists momentarily after a non-central collision) was reconstructed using the charged particles and free neutrons. Thus, the reconstruction includes determination of the QP composition, both A and Z . In order to select thermally equilibrated QPs, the QPs are required to be on-average spherical, in a narrow range of shape deformation. The excitation energy of the QPs is determined from the transverse kinetic energy of the charged particles, the Q -value of the QP breakup, the neutron multiplicity, and average neutron kinetic energy. This method of reconstruction has previously been described in detail [36,49,50,51,52,53,54]. In this way, a set of quasi-projectiles was obtained, tightly selected on mass ($48 \leq A_{QP} \leq 52$), and which have properties consistent with thermal equilibration (i.e. selected on minimal shape deformation), and with known neutron-proton asymmetry.

4.2 Thermodynamic parameter determination

The characterization of properties of this low density matter necessarily begins with the determination of the temperature and density regions actually sampled in the collision. Temperature determinations are relatively well in hand as there is a long history of experiments focusing on temperature determination which we will not repeat here. See for example [43,51,52,55,56,57,58,59,60,61,62,63,64,65,66,67,68,69,70,71]. In the work described in the following we have employed the Albergo method [72] which uses double isotope ratios to determine temperatures based on chemical equilibrium assumptions. Thus, temperatures are determined using a H-He thermometer based on the double yield ratio of deuterons, tritons, ^3He and ^4He . Another method to extract temperatures is the analysis of fluctuations in the transverse momentum [73].

Accurate density determinations are inherently more difficult. Among the different experimental approaches which have been explored to extract densities for systems below normal density are:

- the use of the Albergo NSE based relations [5,72],
- the use of the Mekjian coalescence model which takes into account three body terms which might mimic either a higher density (three body collisions) or Pauli blocking [39,74],
- analyses of caloric curve data or barrier data within the Fermi-Gas Model framework [75,76],
- the quantum fluctuation analysis method [73],
- an approach based on use of the Chemical equilibrium constant employed in Ref. [39].

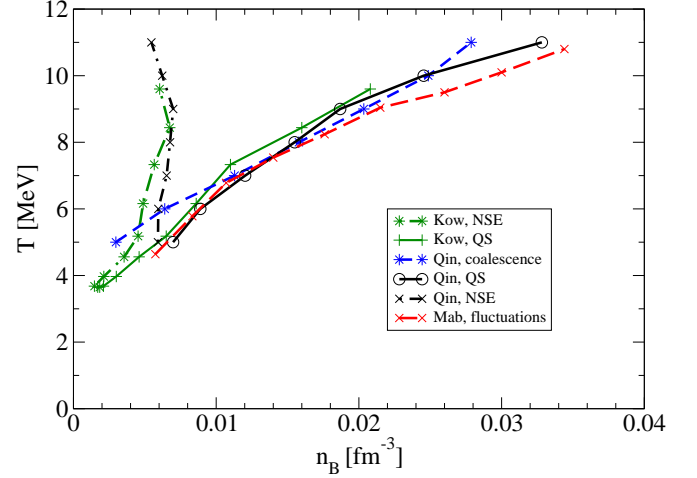


Fig. 5. Baryon density derived from yields of light elements. Data according to [5] (Kow) [39], (Qin) [73], (Mab) are compared with the results of the analysis of yields using NSE and QS calculations for $K_c(\alpha)$.

The last approach was described in a recent paper [77]. The yields of d , t , ^3He and ^4He for evolving intermediate source systems formed in the collisions of $47A$ MeV ^{40}Ar with ^{112}Sn and ^{124}Sn , and $47A$ MeV ^{64}Zn with ^{112}Sn and ^{124}Sn were determined and this technique was applied to determine densities and temperatures. The free neutron yields are not measured but are determined from the free proton yield and the yield ratio of ^3H to ^3He . To determine the asymmetry parameter of the emitting sources the total proton and neutron yields including those bound in clusters are used. Values of $n = 0.002 - 0.032$ nucleons/ fm^3 and $T = 5 - 10$ MeV were obtained. Figure 5, taken from that work [77], shows these results compared to results from several other analyses [5,39,73]. While the NSE model is applicable at only very low densities, below $n \approx 0.001 \text{ fm}^{-3}$ [78], the other models employed significantly higher densities and exhibit very reasonable agreement with each other.

The comparison of results from different techniques of extracting T and n_B from experimental data are presented in Fig. 5. Interestingly, the results of the coalescence model analysis [39] and the quantum fluctuation analysis [73] presented in Fig. 5 lead to very similar results. Both produce results quite similar to the densitometer analysis based on calculated QS model equilibrium constants. The fact that the two different experimental results for the temperature and density regions explored are consistent with each other despite the fact that they are obtained from quite different beam energies, emitting sources and analyses, suggests that an underlying unifying feature of the EOS is responsible. Indeed, further analysis by Mabilia *et al.* [50,51,73] indicate that the data are sampling the vapor branch of the liquid gas coexistence curve and may be employed to determine the critical tempera-

tures of mesoscopic nuclear systems, within the framework of the Guggenheim systematics, in a manner analogous to previous treatments [75,79].

4.3 Test of the nuclear matter EOS at low densities

With our confidence in the temperature and density determinations bolstered by the consistency exhibited in Fig. 5, we have addressed various aspects of clustering in the low density nuclear matter produced. In theoretical models cluster mass fractions are commonly used to characterize the degree of clusterization in low density matter. However, different theoretical models include various different competing species. This leads to differences in particular mass fractions quoted. If all relevant species are not included in the calculation, mass fractions cannot be accurately determined. To avoid this problem we have proposed that equilibrium constants for cluster formation be employed instead of mass fractions. In contrast to mass fractions, cluster formation equilibrium constants, such as that for α particle formation, i.e.,

$$K_c(\alpha) = \frac{n_\alpha}{n_n^2 n_p^2} \quad (39)$$

where n_α , n_n , and n_p are the α particle, neutron and proton densities, respectively, should be independent of proton fraction and choice of competing species.

Figure 6 from reference [39] depicts a comparison between our experimentally derived equilibrium constants and those resulting from models employing a variety of equations of state proposed for astrophysical applications [8,9,10,11,16].

Not surprisingly the calculated values of the equilibrium constant tend to converge at the lower densities. Even at the lowest densities sampled, however, there are significant differences. At higher densities, 0.01 to 0.03 nuc/fm^3 , the various interactions employed all lead to a decrease of K_c below that of the Nuclear Statistical Equilibrium (NSE) values of Typel *et al.* [16], as expected. However most of them lead to higher values of $K_c(\alpha)$ than those derived from the experiment. The Lattimer-Swesty model [8] using Skyrme models with incompressibilities of 180 and 220 MeV and employing an excluded volume technique predict values slightly higher than the experimental values. This is also true for the Statistical Equilibrium model of Hempel and Schaffner-Bielich using an NL-3 interaction and also employing an excluded volume technique [11]. The Quantum Statistical Model of Röpke *et al.*, which includes the medium modifications of the cluster binding energies leads to values close to the experimental values [24,32]. The data provide important new constraints on the model calculations.

4.4 Shift of the binding energies and Mott points

Using the equilibrium constants it is possible to derive temperature and density dependent binding energies of

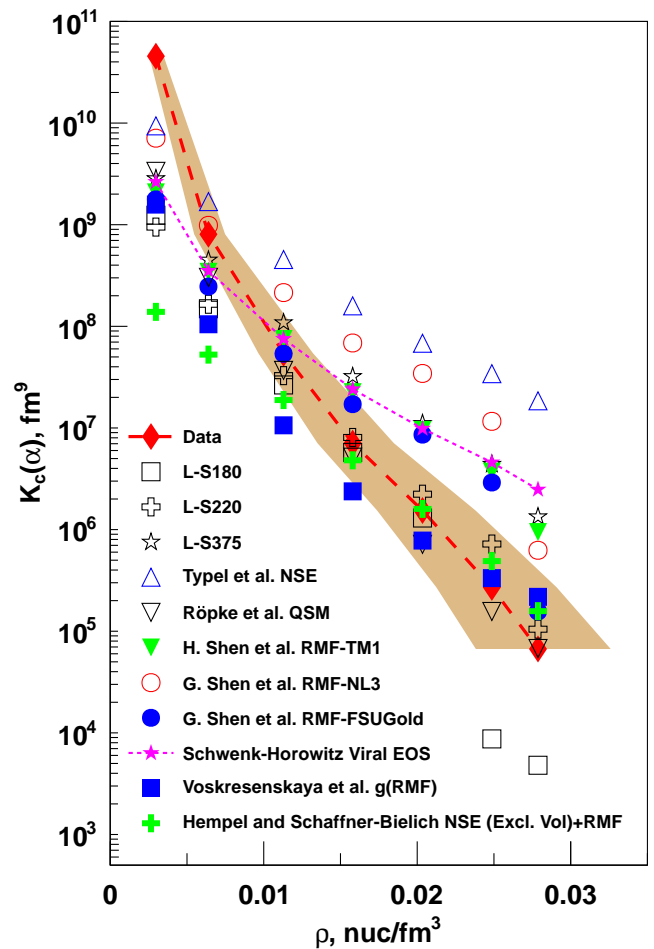


Fig. 6. Comparison of experimental values of $K_c(\alpha)$ with those from various EOS calculations [39].

$d, t, {}^3\text{He}$ and α clusters from the data [80]. Since the observed temperatures and densities are correlated in our experiment the point at which an experimentally derived cluster binding energy is zero with respect to the surrounding medium corresponds to a particular combination of density and temperature. Thus, for our data, on clusters produced in collisions of 47 A MeV ${}^{40}\text{Ar}$ and ${}^{64}\text{Zn}$ projectiles with ${}^{112}\text{Sn}$ and ${}^{124}\text{Sn}$ target nuclei we are able to extract a single Mott point for each cluster. In Figure 7 we present the values of the Mott temperatures and densities and compare them with the loci of the values of medium modified binding energies predicted by the thermodynamic Green's function method [24,32], see Typel *et al.* [16]. This approach makes explicit use of an effective nucleon-nucleon interaction to account for medium effects on the cluster properties. We see that the agreement between the predictions and the experimental results is quite good.

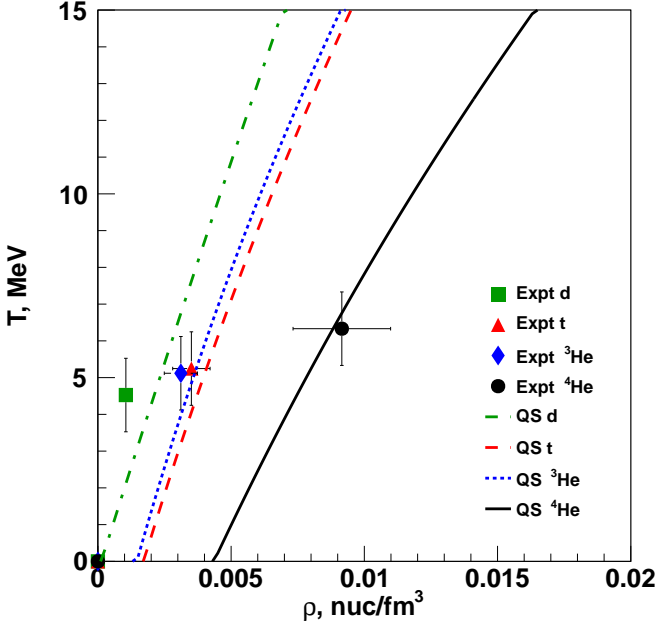


Fig. 7. Comparison of experimentally derived Mott point densities and temperatures with theoretical values [80]. Symbols represent the experimental data. Estimated errors on the temperatures are 10 % and on the densities 20 %. Lines show polynomial fits to the Mott points presented in reference [16].

5 Clusterization and the Symmetry Energy at Low Nucleon Density

5.1 Isoscaling and free symmetry energy

To explore the symmetry energy in low density nuclear matter we first employed isoscaling techniques to derive symmetry free energies [81]. This analysis assumes that for two systems with similar temperatures but different N/Z ratios, the ratio of yields of a particular isotope of mass number A , proton number Z , and neutron number N in the two systems may be expressed as [82,83]

$$\begin{aligned} \frac{Y_2(Z, N)}{Y_1(Z, N)} &= C e^{(\mu_2(n) - \mu_1(n))N + (\mu_2(p) - \mu_1(p))Z} / T \\ &= C e^{\alpha N + \beta Z}, \end{aligned} \quad (40)$$

where C is a constant and $\mu(n)$ and $\mu(p)$ are the neutron and proton chemical potentials. The isoscaling parameters $\alpha = (\mu_2(n) - \mu_1(n))/T$ and $\beta = (\mu_2(p) - \mu_1(p))/T$, representing the difference in chemical potential between the two systems, may be extracted from suitable plots of yield ratios. Either parameter may then be related to the symmetry free energy, F_{sym} . We take the α parameter, which is expected to be less sensitive to residual Coulomb effects. With the usual convention that system 2 is richer in neutrons than system 1,

$$\alpha = 4F_{\text{sym}} \left[\left(\frac{Z_1}{A_1} \right)^2 - \left(\frac{Z_2}{A_2} \right)^2 \right] / T, \quad (41)$$

where Z is the atomic number and A is the mass number of the emitter [41,82,83]. Thus, F_{sym} may be derived directly from determinations of system temperatures, Z/A ratios, and isoscaling parameters. We emphasize that the present analysis is carried out for light species characteristic of the nuclear gas rather than, as in most previous analyses, for the intermediate mass fragments thought to be characteristic of the nuclear liquid.

In this work we employ Eq. (40) with experimentally determined isoscaling parameters, α , temperatures, T , and Z/A ratios to determine the symmetry free energy coefficient F_{sym} . Assuming the quadratic behavior of the symmetry energy term in the mass formula we can write $\alpha = 4F_{\text{sym}} \Delta(Z/A)^2 / T$. Here α is the isoscaling coefficient determined from yield ratios of $Z = 1$ ejectiles of the two reactions, F_{sym} is the free symmetry energy and $\Delta(Z/A)^2$ is the difference of the squared asymmetries of the sources in the two reactions.

The isoscaling analysis has been employed (as a function of v_{surf}) to determine α via the expression (40). With $\Delta(Z/A)^2$ and the temperature determined from observed yields, the free symmetry energy is extracted [5,40].

5.2 Internal symmetry energy

From the free symmetry energy F_{sym} the internal symmetry energy E_{sym} can be derived if the symmetry entropy S_{sym} is known,

$$E_{\text{sym}} = F_{\text{sym}} + T S_{\text{sym}}. \quad (42)$$

Simple approximations for S_{sym} obtained from NSE or virial expansions, see [5], cannot be used to derive the symmetry energy from the free symmetry energy. Given the general consistency of our data with the results of the QS calculations we have employed that model to determine the requisite symmetry entropies as a function of density and temperature. In contrast to the mixing entropy that leads to a larger entropy for uncorrelated symmetric matter in comparison with pure neutron matter, the formation of correlations, in particular clusters, will reduce the entropy in symmetric matter, see Fig. 10 of Ref. [16]. For parameter values for which the yields of free nucleons in symmetric matter are small, the symmetry entropy may become positive for low temperatures. The fraction of nucleons bound in clusters can decrease, e.g. due to increasing temperature or the dissolution of bound states at high densities due to the Pauli blocking. Then, the symmetric matter recovers its larger entropy so that the symmetry entropy becomes negative.

Within this analysis we have employed the calculated symmetry entropy coefficients from the QS model [40,41] to determine the entropy contribution to the symmetry free energy and extract values of the symmetry energy coefficients from the data. The symmetry energies derived in this manner are presented in Fig. 8.

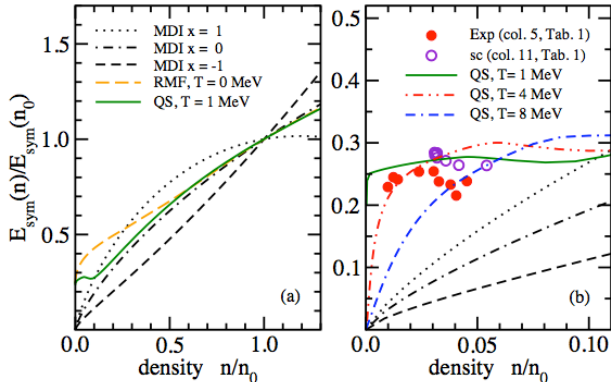


Fig. 8. Comparisons of the scaled internal symmetry energy $E_{\text{sym}}(n)/E_{\text{sym}}(n_0)$ as a function of the scaled total density n/n_0 for different approaches and the experiment. (left panel): The commonly used MDI parametrization of Chen *et al.* [84] for $T = 0$ and different asy-stiffnesses, controlled by the parameter x (dotted, dot-dashed and dashed (black) lines). The result of the QS calculation including light clusters for temperature $T = 1$ MeV is shown as the solid (green) line. We also show the symmetry energy for a RMF calculation at $T = 0$ where heavy clusters have been included (long-dashed (beige) line). (right panel): The internal scaled symmetry energy in an expanded low-density region. Shown are again the MDI curves and the QS results for $T = 4$ and 8 MeV. We compare these with the experimental data with the NSE entropy (solid circles) and the results of the self-consistent calculation (open circles) from Ref. [41]. Recall that both T and n vary for the experimental data.

5.3 Results for the symmetry energy and discussion

The derived symmetry energy coefficients are plotted against density in Figure 8 where they are compared to those which are predicted by the RMF and QS model calculations [3]. Note that the underlying RMF model for the quasiparticle description with $n_0 = 0.149 \text{ fm}^{-3}$, $E_{\text{sym}}(n_0) = 32.73 \text{ MeV}$ gives a reasonable behavior at high density. However, at the lowest densities sampled the quasiparticle mean-field approach (RMF without clusters) disagrees strongly with the experimentally deduced symmetry energy while the QS approach gives a rather good agreement with the experimental data. This reflects the formation of clusters, primarily α particles, not included in such calculations. The model with medium effects describes quite well the low-density symmetry energy data that were extracted from our analysis of heavy-ion collisions.

In Fig. 8 we compare the internal symmetry energy in different approaches with the experimental values. In the left panel of the figure we show theoretical results for T at or close to zero. A widely used momentum-dependent parametrization of the symmetry energy (MDI) at temperature $T = 0$ MeV was given in Refs. [1, 84] and is shown by dotted, dot-dashed and dashed lines corresponding to

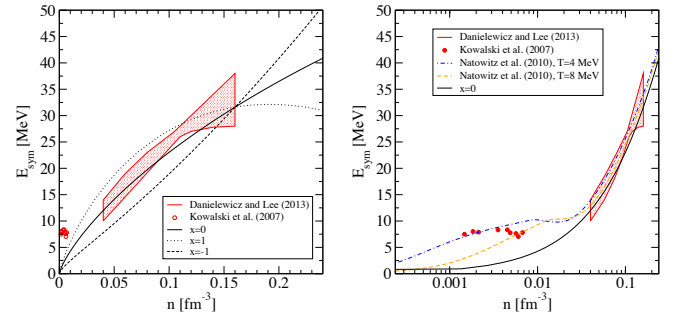


Fig. 9. Symmetry energy as function of density, linear scale (left panel) and logarithmic scale (right panel). Experiment [5] compared with predictions according to the MDI parametrization of Chen *et al.* [84] with different parameter values x and the QS model [41]. The hatched area shows constraints obtained from Isobaric Analog States (IAS) of Danielewicz and Lee [85]. Courtesy of David Blaschke.

different values of the stiffness, governed by the parameter x . However, all these parametrizations vanish in the low-density limit. We compare this to the QS result at $T = 1$ MeV (since the QS approach is not suitable for constructing the correlated ground state at $T = 0$). In this approach the symmetry energy is finite at low density. (Because of the finite temperature at extremely low densities of the order of 10^{-5} fm^{-3} this curve will also approach zero.) Also note that the underlying RMF model for the quasiparticle description gives a reasonable behavior at high density similar to the MDI, $x=0$ parametrization. We thus see that the QS approach successfully interpolates between the clustering phenomena at low density and a realistic description around normal density. The generalized RMF, $T = 0$ curve (see [16]) was constructed taking into account cluster formation, but demands further discussion with respect to the treatment of Coulomb interaction and phase transitions, see [3].

Fig. 9 shows a comparison of the symmetry energy extracted from experimental data [5] to predictions of Danielewicz and Lee [85] and Chen *et al.* [84]. The hatched area in the figure shows constraints obtained from analysis of isobaric analog states [85]. Calculations in [41] combined with this analysis suggest a smooth transition from low density to normal nuclear density.

In the right panel of Fig. 8 as well as in Fig. 10 we compare the internal symmetry energy derived from the experimental data [5, 40, 41] in an expanded low-density region with the RMF and QS results. Again, it is clearly seen that the quasiparticle mean-field approach (RMF without clusters) disagrees strongly with the experimentally deduced symmetry energy while the QS approach gives a rather good agreement with the experimental data.

We find that medium-dependent cluster formation has to be considered in theoretical models to obtain the low-density dependence of the symmetry energy that is observed in experiments. The frequently used presentation for the density dependence of the symmetry energy that

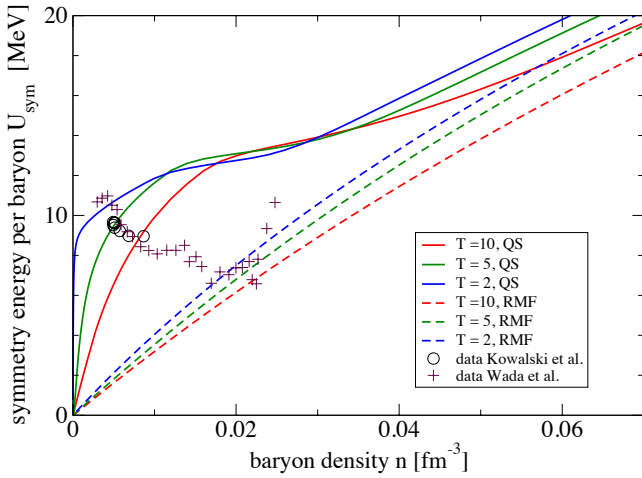


Fig. 10. Internal symmetry energy coefficients as a function of baryon density in nucleons/ fm^3 . Experimental results [5,40] are compared to results of QS model calculations, see Fig. 8. For the experimental data, T varies in the region 3 - 11 MeV, see [40,41].

show vanishing symmetry energy at zero density and an increase that is linear with the density is not correct because correlations and cluster formation are essential in the low-density region. Note the strong dependence on temperature that is also not considered in the standard presentations, but has to be taken into account for applications in astrophysics and heavy ion collisions where temperatures in the range of several MeV are of interest.

6 Conclusion and outlook

In conclusion, our comparison of experimental data with results of model calculations strongly indicates that accurate modeling of clusterization in low density matter is critical for both nuclear and astrophysical applications. A quantum-statistical model of nuclear matter, that includes the formation of clusters at densities below nuclear saturation, describes quite well the experimental low-density symmetry energy which was extracted from the analysis of heavy-ion collisions.

Using the QS approach, the composition and the thermodynamic quantities of nuclear matter can be modeled over a large region of densities, temperatures and asymmetries. In particular, it reproduces the statistical models of a gas consisting of various nuclei at low densities and the mean-field approaches that are applicable near the saturation density. An important ingredient is the disappearance of bound states at a certain density (denoted as Mott density) due to Pauli blocking.

Analyzing heavy ion collisions using the NIMROD multi-detector at the Cyclotron Institute at Texas A & M University the medium modification of light fragments that

leads to the dissolution has been shown. Yields of light particles produced in the collisions of $47 A$ MeV ^{40}Ar with ^{112}Sn , ^{124}Sn and ^{64}Zn with ^{112}Sn , ^{124}Sn were employed in thermal coalescence model analyses to derive densities and temperatures of the evolving emitting systems. The nuclear matter equation of state has been tested, and significant deviations from the NSE have been found. The relevance of medium modifications that are obtained from the QS approach have been proven by experiments.

Isoscaling analyses were used to determine the free symmetry energies of these systems. Comparisons of the experimental values with those of calculations made using a model which incorporates medium modifications of cluster binding energies reveal a very good agreement. The model calculated symmetry entropies have been used together with the experimental free symmetry energies to derive symmetry energies of nuclear matter at densities of $0.03 \leq n/n_0 \leq 0.2$ and temperatures in the range 5 to 11 MeV. It has been shown that the occurrence of bound states, absent in a mean-field approach, leads to a significant increase of the symmetry energy in the low-density region in contrast to a linear increase of the symmetry energy with density as predicted by many mean-field motivated models. In the low-density region, the symmetry energy is strongly depending on temperature.

Acknowledgement: This research was supported by CompStar, a Research Networking Programme of the European Science Foundation, and in particular by grant No. DE-FG03-93ER40773 (Texas A & M) and by Robert A. Welch Foundation grant No. A0330 (JBN).

References

1. B. A. Li, *et al.*, Phys. Rept. **464**, 113 (2008).
2. J. M. Lattimer and M. Prakash, Phys. Rep. **442**, 109 (2007).
3. S. Typel *et al.*, this volume
4. K. Sumiyoshi and G. Röpke, Phys. Rev. C **77**, 055804 (2008).
5. S. Kowalski *et al.*, Phys. Rev. C **75**, 014601 (2007).
6. E. O'Connor and C. D. Ott, Class. Quant. Grav. **27**,114103 (2010).
7. E. J. Lentz *et al.*, J. Astrophys. **760**, 94 (2012).
8. J. M. Lattimer, *et al.*, Nucl. Phys. A **A535**, 331 (1991).
9. H. Shen *et al.*, Nucl. Phys. **A637**, 435 (1998).
10. G. Shen *et al.*, arXiv:nucl-th/1101.3715 (2011)
11. M. Hempel *et al.*, Nucl. Phys. **A837**, 210 (2010).
12. C. J. Horowitz and A. Schwenk, Nucl. Phys. **A776**, 55 (2006).
13. D. Lunney, J.M. Pearson, and C. Thibault, Rev. Mod. Phys. **75**, (2003) 1021-1082.
14. P. Danielewicz, Nucl. Phys. **A727**, 233 (2003).
15. H. Jiang, *et al.*, Phys. Rev. C **85**, 024301 (2012).
16. S. Typel, G. Röpke, T. Klähn, D. Blaschke and H. H. Wolter, Phys. Rev. C **81**, 015803 (2010).
17. W.-D. Kraeft, D. Kremp, W. Ebeling and G. Röpke, *Quantum Statistics of Charged Particle Systems*, Akademie-Verlag, Berlin, 1986.
18. C. Fuchs and H. H. Wolter, Eur. Phys. J. **A30**, 5 (2006).
19. T. Klähn *et al.*, Phys. Rev. C **74**, 035802 (2006).

20. G. Watanabe, *et al.*, Phys. Rev. Lett. **103**, 121101 (2009).
21. G. Röpke *et al.*, Nucl. Phys. **A379**, 536 (1982); **A424**, 594 (1984).
22. M. Schmidt, G. Röpke, and H. Schulz, Ann. Phys. (N.Y.) **202**, 57 (1990).
23. J. P. Bondorf, *et al.*, Phys. Rept. **257**, 133 (1995).
24. G. Röpke, Phys. Rev. C **79**, 014002 (2009).
25. S. Typel, Phys. Rev. C **71**, 064301 (2005).
26. G. Röpke, N.-U. Bastian, D. Blaschke, T. Klähn, S. Typel, and H. H. Wolter, Nucl. Phys. **A897**, 70 (2013).
27. D. Vautherin and D. M. Brink, Phys. Lett. **B32**, 149 (1970); Phys. Rev. C **5**, 626 (1972).
28. G. Röpke, A. Grigo, K. Sumiyoshi, and Hong Shen, Phys. Part. Nucl. Lett. **2**, 275 (2005).
29. G. Röpke, M. Schmidt and H. Schulz, Nucl. Phys. **A424**, 594 (1984).
30. A. Kolomiets *et al.*, Phys. Rev. C **55**, 1376 (1997).
31. S. Shlomo and V. M. Kolomietz, Rep. Prog. Phys. **68**, 1 (2005).
32. G. Röpke, Nucl. Phys. **A867**, 66 (2011).
33. G. Röpke *et al.*, Phys. Stat. Sol. (b) **100**, 215 (1980).
34. V. Baran, *et al.*, Phys. Rept. **410**, 335 (2005).
35. M. B. Tsang *et al.*, Phys. Rev. Lett. **102**, 122701 (2009).
36. S. Wuenschel *et al.*, Phys. Rev. C **79**, 061602(R) (2009).
37. C. Sfienti, *et al.*, Phys. Rev. Lett. **102**, 152701 (2009).
38. J. Wang *et al.*, Phys. Rev. C **75**, 014604 (2007).
39. L. Qin *et al.*, Phys. Rev. Lett. **108**, 172701 (2012).
40. R. Wada *et al.*, Phys. Rev. C **85**, 064618 (2012).
41. J. B. Natowitz *et al.*, Phys. Rev. Lett. **104**, 202501 (2010).
42. S. Wuenschel *et al.*, Nucl. Instrum. Methods Phys. Res. **A604**, 578 (2009).
43. K. Hagel *et al.*, Phys. Rev. C **62** 034607 (2000)
44. L. Qin, Thesis, Texas A&M University (2008).
45. J. Wang *et al.*, Phys. Rev. C **72**, 024603 (2005).
46. Z. Kohley *et al.*, Phys. Rev. C **86**, 044605 (2012)
47. Z. Kohley *et al.*, Phys. Rev. C **83**, 044601 (2011)
48. A.B. McIntosh *et al.*, *How Much Cooler Would It Be With Some More Neutrons?*, this volume
49. S. Wuenschel, Ph.D. thesis, Texas A & M Univ. (2009)
50. A.B. McIntosh *et al.*, Phys. Lett. **B719**, 337 (2013)
51. A.B. McIntosh *et al.*, Phys. Rev. C **87**, 034617 (2013)
52. S. Wuenschel *et al.*, Nucl. Phys. **A843**, 1 (2010)
53. P. Marini *et al.*, Phys. Rev. C **85**, 034617 (2012)
54. J.C. Steckmeyer *et al.*, Nucl Phys. **A686**, 537 (2001)
55. G. Nebbia *et al.*, Phys. Lett. **B176**, 20 (1986).
56. H. M. Xu *et al.*, Phys. Lett. **B182**, 155 (1986).
57. D. Fabris *et al.*, Phys. Lett. **B196**, 429 (1987).
58. K. Hagel *et al.*, Nucl. Phys. **A486**, 429 (1988).
59. R. Wada *et al.*, Phys. Rev. C **39**, 497 (1989).
60. M. Gonin *et al.*, Phys. Lett **B217**, 406 (1989).
61. A. Chbihi *et al.*, Phys. Rev. C **43**, 666 (1991).
62. T. K. Nayak *et al.*, Phys. Rev. C **45**, 132 (1992).
63. C. Schwarz *et al.*, Phys. Rev. C **48**, 676 (1993).
64. J. B. Natowitz *et al.*, Phys. Rev. C **52**, R2322 (1995).
65. M. B. Tsang *et al.*, Phys. Rev. C **53**, R1057 (1996).
66. Z. Majka *et al.*, Phys. Rev. C **55**, 2291, (1997).
67. M. J. Huang *et al.*, Phys. Rev. Lett. **78**, 1648 (1997).
68. H. Xi *et al.*, Phys. Lett. **B431**, 8 (1998).
69. H. Xi *et al.*, Phys. Rev. C **59**, 1567 (1999).
70. J. B. Natowitz *et al.* Phys. Rev. C **65**, 034618 (2002).
71. S. R. Souza *et al.*, Phys. Rev. C **80**, 044606 (2009).
72. S. Albergo, *et al.*, Nuovo Cimento A **89**, 1 (1985)
73. H. Zheng and A. Bonasera, Phys. Lett. B **696**, 178 (2011); H. Zheng, G. Giuliani, and A. Bonasera, Nucl. Phys. A **892**, 43 (2012); J. Mabilia *et al.*, arXiv:1208.3480v1 [nucl-ex].
74. A. Z. Mekjian, Phys. Rev. C **17**, 1051 (1978); Phys. Rev. Lett. **38**, 640 (1977).
75. J. B. Natowitz *et al.*, Int. J. Mod. Phys. E **13**, 269 (2004).
76. V. E. Viola *et al.*, Phys. Rev. Lett. **93**, 132701 (2004).
77. G. Röpke *et al.*, Phys. Rev. C **88**, 024609 (2013).
78. S. Shlomo *et al.*, Phys. Rev. C **79**, 034604 (2009).
79. J. B. Elliott *et al.*, Phys. Rev. C **67**, 024609 (2003); J. B. Elliott *et al.*, arXiv:1203.5132 submitted to Phys. Rev. C (2013).
80. K. Hagel *et al.*, Phys. Rev. Lett. **108**, 062702 (2012).
81. M. B. Tsang *et al.*, Phys. Rev. Lett. **86**, 5023 (2001).
82. M. B. Tsang *et al.*, Phys. Rev. C **64**, 041603 (2001).
83. S. R. Souza *et al.*, Phys. Rev. C **78**, 014605 (2008).
84. L. W. Chen *et al.*, Phys. Rev. Lett. **94**, 032701 (2005); Phys. Rev. C **76**, 054316 (2007).
85. P. Danielewicz and J. Lee, arXiv:1307.4130 [nucl-th]